Invasion percolation on self-affine topographies

G. Wagner, P. Meakin, J. Feder, and T. Jøssang
Department of Physics, University of Oslo, Box 1048, Blindern, 0316 Oslo 3, Norway
(Received 12 August 1996)

Invasion percolation (IP) with trapping was studied on two-dimensional substrates with a correlated distribution of invasion thresholds. The correlations were induced by using the heights of (2+1)-dimensional self-affine rough surfaces with Hurst exponents in the range $0<H<1$ to assign the threshold values. The resulting IP clusters consist of ''blobs'' with sizes up to the entire cluster size that are connected by fine ''threads.'' The fractal dimensionality D_H of the IP clusters is dominated by the blobs. The blob size distribution is is related to H and D_H. [S1063-651X(97)11401-5]

PACS number(s): 47.55.Mh, 47.60.+i, 05.40.+j

I. INTRODUCTION

The invasion percolation (IP) algorithm [1–3] is remarkably successful in describing the slow immiscible displacement of a wetting fluid by a nonwetting fluid in a porous media [4–10]. In slow displacements, viscous forces can be neglected, and the process is governed by the capillary forces. In equilibrium, the pressure of the nonwetting fluid must exceed the pressure of the wetting fluid by an amount p_c, the capillary pressure, to sustain the curvature of the interface. When a nonwetting fluid is injected into a pore filled with wetting fluid, the capillary pressure must be overcome. For a circular throat of radius R and for the interfacial tension Γ acting between the two fluids, $p_c=-2\Gamma\cos\theta/R$, where θ is the contact angle. The contact angle denotes the angle at which the interface between the two phases meets the solid surface of the matrix. Thus the nonwetting fluid preferentially invades the pores with the largest throats.

The displacement process can be mapped on the IP model in a straightforward manner. In site IP, the porous medium is represented by a lattice of sites. Each site i is assigned a random number r_i, and represents a pore with the diameter $1/r_i$. Initially, all sites are occupied by the wetting ''defender'' fluid. An injection site is chosen and filled with the nonwetting ''invader'' fluid. The algorithm consists of repeating the following three steps: (1) Identify all defender sites that are adjacent to the invaded sites. (2) Among these perimeter sites, find the one with the lowest number r_i. (3) Fill this site with an invader fluid. The process is terminated when the edge of the lattice is reached by the cluster formed by the invader fluid.

In two dimensions, the incompressibility of the two fluids must be taken into account by using a ''trapping rule'' [3]. When the invader fluid has surrounded a region of defender fluid, the defender fluid cannot be displaced, and is trapped. Growth of the IP cluster must take place at unoccupied perimeter sites that are not trapped, i.e., a path consisting of steps between nearest-neighbor unoccupied sites to the outside of the cluster must exist. The trapping rule appears to change the universality class of the model.

In standard IP, the thresholds are distributed uniformly on the unit interval without any spatial correlation in their values, representing a homogeneous porous medium. However, the pore sizes in geological fields clearly are strongly correlated on large scales, and there are indications that correlations also exist on scales down to the pore scale [11]. Motivated by this observation, the IP model with and without trapping was studied using a multifractal distribution of thresholds [12,13]. In these studies the fractal dimensionality of the IP cluster was reported to be little or not at all affected by the spatial correlations. In contrast, changes in the IP cluster growth pattern were observed in simulations using site-bond lattices in which correlations were induced by the constraint that a bond size be less than or equal to the size of the smaller site to which it was connected [14].

In the present work, IP with trapping in two dimensions was studied using substrates with a different kind of correlated disorder. For each site i at the position (x_i,y_i) in a two-dimensional lattice of $L\times L$ sites, the threshold value assigned to the site was given by the z value of a rough surface $z(x_i,y_i)$ with the same extension $L\times L$ in the x-y plane. The substrate obtained in this way may be used to model the slow displacement of a wetting fluid in a fracture by a nonwetting fluid. The three-dimensional fracture is represented by the two-dimensional lattice such that each lattice site corresponds to a region of the fracture plane, and the threshold r_i assigned to the site corresponds to the aperture of the fracture.

For a perfectly nonwetting fluid ($\theta=180°$) to advance and displace a wetting fluid in a fracture region of infinite extension and of aperture a, the capillary pressure

$$p_c=\frac{2\Gamma}{a} \tag{1}$$

must be overcome. The nonwetting fluid tends to invade fracture regions with wide apertures, and does not displace the wetting fluid from narrow aperture regions. In the quasistatic case, the displacement process is governed entirely by the fracture geometry.

Field measurements of natural rock surfaces indicate a fractal character [15–18]. Fresh brittle fractures of different types of rock were shown to generate self-affine rough surfaces [19]. An isotropic self-affine surface $z(x,y)$ remains statistically invariant to the scaling transformation $x\to\lambda x$, $y\to\lambda y$, and $z\to\lambda^H z$. The roughness exponent or Hurst exponent H lies in the range $0<H<1$. For $H=0.5$, a ''vertical'' cross section of the surface has the same statistical

properties as a Brownian process. For $H>0.5$, the cross section is persistent (segments leading in the positive or the negative z direction are likely to be followed by segments leading into the same z direction), and for $H<0.5$, the surface is antipersistent. For $H\neq 0.5$, the cross section is characterized by a process called fractional Brownian motion [20]. A simple model of a fracture aperture field $a(x,y)$ is provided by taking the difference of two self-affine surfaces $z_1(x,y)$ and $z_2(x,y)$ (with the same amplitude and roughness exponent) representing the fracture boundaries,

$$a(x,y)=z_2(x,y)-z_1(x,y). \tag{2}$$

As long as the surfaces do not overlap $[a(x,y)>0]$, the invasion thresholds r_i are well defined after discretizing the aperture field $a(x,y)$ on a lattice of sites. The aperture field also forms a self-affine surface with the same roughness exponent as the two surfaces [21]. In the present work, aperture fields were modeled by the z-value fields $z(x,y)$ of single self-affine surfaces:

$$a(x,y)=z(x,y). \tag{3}$$

Invasion percolation using this type of substrates was also studied recently by Paterson *et al.* [22] and Du, Satik, and Yortsos [23]. Percolation on self-affine topographies was applied by Sahimi [24] to model transport phenomena in heterogeneous media. Invasion percolation in three dimensions, using heterogeneous substrates characterized by fractional Brownian motion, was studied by Paterson and Painter [25].

II. SIMULATION

Periodic self-affine surfaces $z(x_i,y_i)$ were generated on a square lattice using a random midpoint displacement algorithm with random successive addition [26,27]. The Hurst exponent characterizing the surfaces was measured using the height difference correlation function

$$\Delta(r)=\langle |z(x_i,y_i)-z(x_i+r_x,y_i+r_y)|^2\rangle_{r_x^2+r_y^2=r^2}. \tag{4}$$

For self-affine surfaces with positive Hurst exponent H, the correlation function scales as $\Delta(r)\sim r^{2H}$ [26]. The invasion threshold fields $r(x_i,y_i)=z(x_i,y_i)$ were obtained from the substrates. All sites on the lattice were filled with the wetting fluid, and the central site of the lattice was filled with the nonwetting fluid. The IP simulation was carried out by letting the cluster of nonwetting fluid grow stepwise and invade perimeter sites with the smallest threshold.

Figure 1 shows a series of IP clusters obtained in this manner. For low values of H $(0<H<0.5)$, the clusters were reminiscent of ordinary IP clusters grown on a lattice with uncorrelated invasion thresholds. Numerous regions of defender fluids became trapped, and the distribution of the sizes of the regions followed a power law.

For higher values of H $(0.5<H<1)$, the clusters had a disordered shape, and could be described in terms of ''blobs'' of different sizes, connected by thin ''threads.'' Compared to the case of low H, a lesser amount of defender fluid became trapped. The IP cluster size distributions were skew, and extended over a large interval. Using $H\approx 0.85$, the largest clusters covered more than 50% of the substrate,

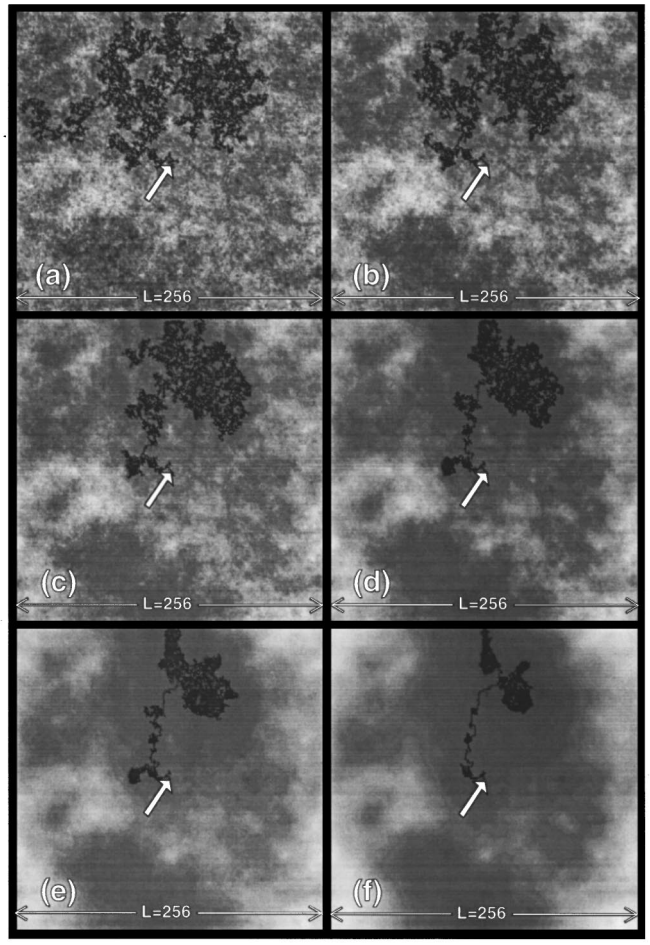

FIG. 1. Clusters of nonwetting fluid (black) obtained from simulations of IP with trapping using self-affine substrates of size $L=256$, at the stage when the edge of the substrate was reached. The grey shade indicates the invasion thresholds used, with bright shades corresponding to high thresholds. For comparison, the random number generator seed was kept constant, and the Hurst exponent was varied from $H=0.13$ (a), $H=0.23$ (b), $H=0.39$ (c), $H=0.55$ (d), $H=0.73$ (e) to $H=0.89$ (f), respectively. The arrow indicates the injection site.

while the smallest ones covered less than 0.005% when the edge of the substrate was reached. In contrast, the size distribution of IP clusters grown on uncorrelated substrates is approximately Gaussian.

A compact blob was formed when the growing IP cluster reached a local threshold minimum M_1 on the substrate, and neighboring sites with higher thresholds were invaded subsequently (see Fig. 2). When the cluster reached a site S separating M_1 from a second local minimum M_2, a thread of invaded sites was formed as the growth of the IP cluster followed a path of steepest descent on the threshold surface. Repeating the cycle, a new blob developed when the region around M_2 was filled out, incorporating an increasing fraction of the thread. Adjacent blobs coalescenced if no further local threshold minima were found. Blobs could thus acquire a size b of the order of the entire cluster size.

III. CLUSTER STRUCTURE AND DIMENSIONALITY

Figure 3 shows, on a log-log scale, the mean number $S(R)$ of cluster sites s counted in a circle of radius R around

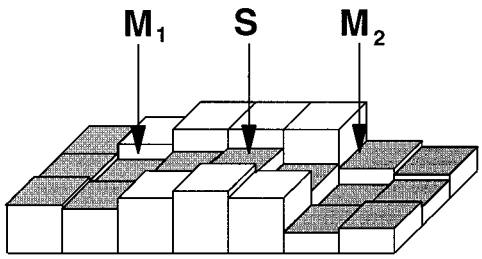

FIG. 2. Illustration of the IP cluster growth model. The invasion threshold of each site i is given by the height $z(x_i, y_i)$ of a rough surface. A blob is formed as the cluster (shaded sites) fills out a region around the local threshold minimum M_1. When the cluster reaches the site S, a thread leading to a second local minimum M_2 is formed. The region around M_2 is then filled.

the center of mass of an IP cluster. The mean size (mass) S is defined by the ratio of the second moment of the size distribution $N(s,R)$ to the first moment, $S=\Sigma s^2 N(s,R)/\Sigma s N(s,R)$. The clusters grew on the correlated substrates using periodic boundary conditions. If a cluster reached the edge of the substrate, it could reenter the substrate from the opposite edge. Each simulation was terminated when a cluster attempted to intersect itself. For a self-similar fractal of fractal dimensionality D,

$$S(R)\sim R^D. \tag{5}$$

In an intermediate range $1<R\ll L$, the measured mean size follows a power law $S(R)\sim R^D$. As a check, D was determined for IP clusters grown on uncorrelated substrates. A linear least-squares fit yielded $D_{\rm uc}=1.82\pm0.01$, consistent with earlier studies of IP [2,3,28,29,13]. Using correlated

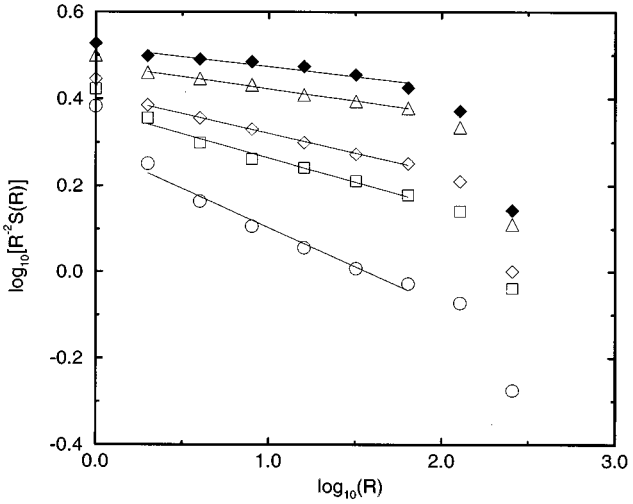

FIG. 3. The dependence of the mean number of sites $S(R)$ in a circle of radius R around the center of gravity of IP clusters, on a log-log scale. $R^{-2}S(R)$ was measured for IP with trapping on uncorrelated substrates (circles) and on correlated substrates with $H\approx0.31$ (squares), $H\approx0.47$ (diamonds), and $H\approx0.85$ (triangles), respectively. $R^{-2}S(R)$ is also plotted for IP without trapping on correlated substrates with $H\approx0.47$ (filled diamonds). The solid lines represent linear least-squares fits for distances in the range $2\leqslant R\leqslant 64$. The substrate size was 512×512 sites.

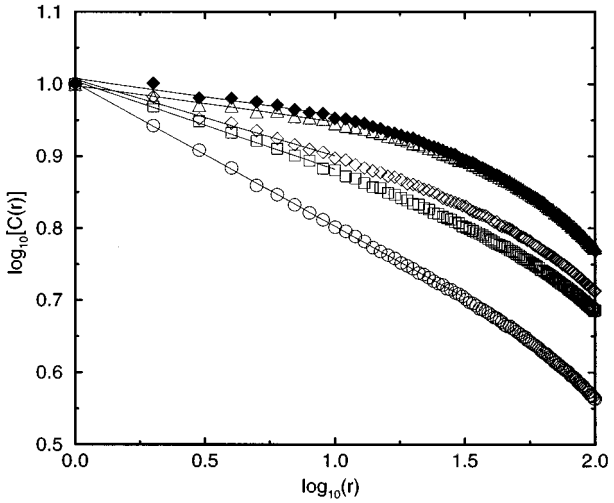

FIG. 4. Log-log plot of the density-density correlation function $C(r)$ versus r, on a log-log scale. $C(r)$ was measured for IP with trapping on uncorrelated substrates (circles) and on correlated substrates with $H\approx0.31$ (squares), $H\approx0.47$ (diamonds), and $H\approx0.85$ (triangles), respectively. Also plotted is $C(r)$ for IP without trapping on correlated substrates with $H\approx0.47$ (filled diamonds). The solid lines represent linear least-square fits to the curves for those values of r where $\log(C(r))$ appears to be a linear function of $\log(r)$. The substrate size was 512×512 sites.

substrates, linear least-squares fits yielded $D_{0.31}=1.89\pm0.01$, $D_{0.47}=1.91\pm0.00$, and $D_{0.85}=1.94\pm0.01$, for $H\approx0.31$, $H\approx0.47$, and $H\approx0.85$, respectively. The errors indicate the standard deviation of the fit parameter. Figure 3 indicates that the IP clusters became more dense as the Hurst exponent increased.

The two-point density correlation function $C(r)$ is frequently used to characterize fractal structures. This quantity is defined as

$$C(r)=\frac{\langle\rho(\mathbf{r}_0)\rho(\mathbf{r}_0+\mathbf{r})\rangle_{|\mathbf{r}|=r}}{\langle\rho(\mathbf{r}_0)\rho(\mathbf{r}_0)\rangle}, \tag{6}$$

where $0\leqslant\rho(\mathbf{r})\leqslant1$ is the cluster mass density and the averaging is over the occupied origins $\mathbf{r}_0$, orientations of the space vector $\mathbf{r}$, and a large sample of clusters. For a self-similar fractal of dimension D on a two-dimensional substrate, $C(r)$ is expected to have the form $C(r)\sim r^{2-D}f(r/r_c)$, where r_c is a distance characteristic of the overall cluster extension. The cutoff function $f(x)$ has the form $f(x)=1$ for $x\ll1$, and decreases faster than any power of x with increasing x for $x\gg1$. Figure 4 shows a plot of $C(r)$, using different values of the Hurst exponent H and the same sample of clusters that was used to measure $S(R)$ (Fig. 3). The correlation function obtained from simulations on uncorrelated substrates shows a decay consistent with $C(r)\sim r^{2-D_{uc}}$ for small r. A linear least-square fit to $C(r)$ yielded $D_{\rm uc}=1.80\pm0.01$. Turning to correlated substrates, linear least-squares fits to $C(r)$ (for $r\ll L$) yielded dimensions of $D_{0.31}=1.88\pm0.01$, $D_{0.47}=1.89\pm0.01$, and $D_{0.85}=1.95\pm0.01$, respectively, for $H\approx0.31$, $H\approx0.47$, and $H\approx0.85$, respectively. These values are consistent with the results presented in Fig. 3 and confirm the systematic increase of the fractal dimensionality of the IP clusters with the degree of spatial correlations.

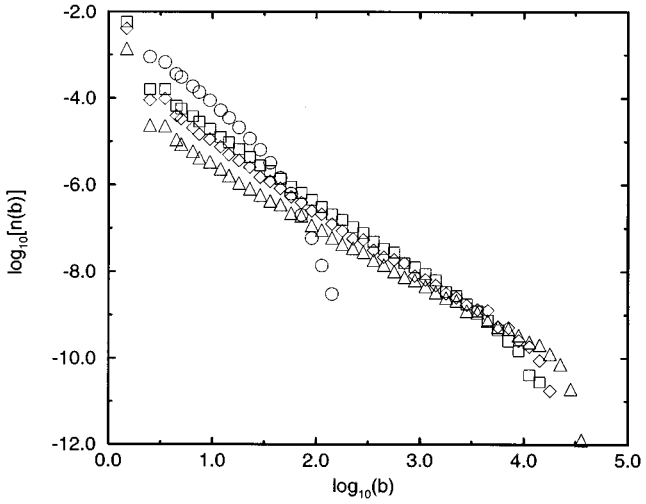

FIG. 5. Log-log plot of the number $n(b)$ of ''blobs'' per lattice site of size b obtained after removing single-connecting cluster sites from IP clusters (with trapping), using a log-log scale. The distributions were averaged over a sample of clusters in bins of logarithmically increasing size. The IP clusters were grown on uncorrelated substrates (circles) and on correlated substates with $H \approx 0.31$ (squares), $H \approx 0.47$ (diamonds), and $H \approx 0.85$ (triangles), respectively. The substrate size was 256×256 sites. Each simulation was terminated when the IP cluster reached the substrate edge.

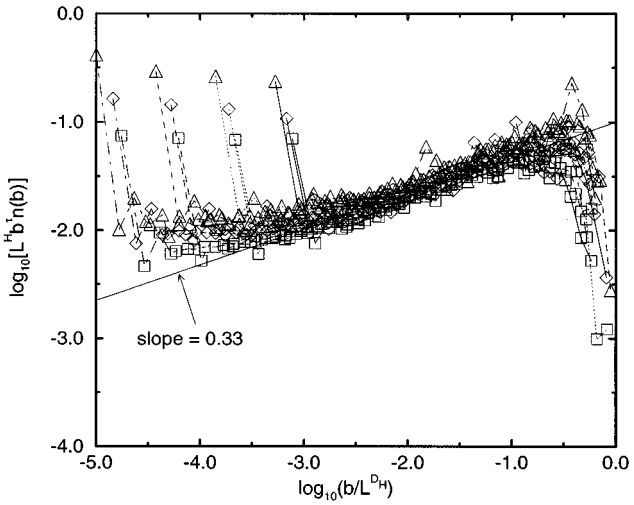

FIG. 6. Attempt to collapse the blob size distributions $n(b)$ measured for IP with trapping onto a single curve by using the scaling form given in Eq.(7). For low values of the argument b/L^{D_H}, the scaling function $f(b/L^{D_H})$ is linear with a slope of approximately 0.33 (straight solid line). The IP clusters were grown on correlated substrates with $H \approx 0.31$ (squares), $H \approx 0.47$ (diamonds), and $H \approx 0.85$ (triangles), respectively. The substrates were of 64×64 sites (solid lines), 128×128 sites (dotted lines), 256×256 sites (dashed lines), and 512×512 sites (dot-dashed lines), respectively. Each simulation was terminated when the IP cluster reached the substrate edge.

The IP cluster structure was studied by measuring the number (per lattice site) $n(b)$ of blobs of size (mass) b obtained by removing the connecting ''threads.'' For each site of an IP cluster, it was determined if the removal of the site fragmented the cluster. In this case, the site was marked as a thread site. When all sites had been tested, the thread sites were removed. The remaining sites defined the blobs. Figure 5 shows the distribution $n(b)$ measured on substrates of 256×256 sites counted at the stage when the growing clusters reached the edge of the substrate. At this stage, cluster sites were removed if the removal implied fragmentation of the IP cluster. The remaining sites defined the blobs. The distributions $n_{L,H}(b)$ of the number of blobs with sizes in the range b to $b+\delta b$ ($\delta b \to 0$) in on a substrate of size L with a Hurst exponent H may be described by the scaling form

$$n_{L,H}(b) \sim L^{-H} b^{-\tau} f(b/L^{D_H}), \tag{7}$$

where $f(x)$ is a scaling function that decreases faster than any power of x for $x \gg 1$. Here the cutoff blob size $b_c \sim L^{D_H}$ was assumed to be equal to the IP cluster size. The exponent τ is given by the size distribution of regions in the self-affine surfaces with a height $z(x,y)$ less than a ''horizontal'' cut parallel to the the x-y plane at an arbitrary height z_0. For self-affine surfaces with $0<H<1$, the linear extension r of such regions scales as $N(r) \sim r^{H-3}$ [20,30]. Making use of Eq. (5), the size distribution of blobs with fractal dimensionality D_H filling out a random sample of regions with $z(x,y)<z_0$ is found to be $N(b) \sim b^{-\tau}$, with $\tau=(2+D_H-H)/D_H$. The L dependence in the scaling form Eq. (7) is obtained from the requirement that the first moment $\mu^{(1)}=\int bn(b)db$ of the blob size distribution scale with the system size as $\mu^{(1)} \sim L^{D_H-2}$. Figure 6 shows an attempt to collapse several blob size distributions $n_{L,H}(b)$ corresponding to different values of L and H on a single curve $f(x)$, using Eq. (7) and the fractal dimensionalities D_H found from the scaling behavior of the mean cluster size. From the figure, the scaling function $f(x)$ is found to be a power law with an exponent of approximately 0.33 for $x \ll 1$.

IV. DISCUSSION

It was recently shown that the percolation transition [31] on a correlated substrate of the type used here is never critical for $H>0$ [32,33]. The percolation exponent ν_H (characterizing the divergence of the correlation length at the percolation threshold) becomes infinite for substrates with topographies given by the z-value field of self-affine surfaces with positive Hurst exponent. On such a substrate, the percolation threshold may be interpreted as the minimal threshold height z_c up to which the underlying self-affine surface must be ''flooded'' (representing the invasion of the corresponding substrate sites) in order to obtain a spanning cluster of flooded regions that are connected to each other. If the relations between critical exponents known from percolation theory carry over, the fractal dimensionality of the infinite percolation cluster at the percolation threshold must be equal to the substrate dimension $d=2$. Du, Satik, and Yortsos [23] measured the density of percolation clusters at the critical threshold on self-affine topographies with $H=0.5$, and reported no dependence on the size of the lattice, implying a cluster dimension of 2. The same result was found earlier by Schmittbuhl, Vilotte, and Roux [32].

There are strong indications that IP without trapping generates a percolation cluster that is equivalent to the infinite percolation cluster [34,35]. IP without trapping thus may be expected to lead to IP clusters with the fractal dimensionality $D_H^\star = 2$. Figures 3 and 4 show attempts to determine the fractal dimensionality for IP without trapping on correlated substrates with $H \approx 0.47$. From the measurement of $S(R)$ in Fig. 3 and $C(r)$ in Fig. 4, $D_{0.47}^\star = 1.95 \pm 0.01$ and $D_{0.47}^\star = 1.95 \pm 0.01$ were obtained, respectively. These results do not permit a definite conclusion since finite-size effects may reduce the effective fractal dimensionality from 2.0 to the measured values of $D_H^\star \approx 1.95$. The IP clusters studied in these measurements had a size between approximately 50 000 and 150 000 sites. This finding may be compared with the fractal codimensionality $\alpha = 2 - D_H^\star = 0.03 \pm 0.01$ measured for $H = 0.5$ in IP without trapping by Paterson *et al.* [22].

Isichenko [30] analyzed the percolation problem on self-affine topographies, and predicted that the perimeter of the infinite percolation cluster is fractal, with a fractal dimensionality $D_H^P = (10 - 3H)/7$ $(0 < H < 1)$. The trapping rule only applies to sites in the interior of the IP clusters, such that the structure of the cluster perimeters is not affected by the rule. IP with trapping may thus lead to IP cluster perimeters that are equivalent to the perimeters of infinite percolation clusters. D_H^P was measured by box counting the perimeters of some of the IP clusters and was found to be consistent with the theoretical prediction.

For IP with trapping, the results presented here indicate that the cluster dimensionality D_H depends on the Hurst exponent H characterizing the threshold correlations of the underlying substrate. Trapping is not a local rule, but affects the growth of the cluster on a global scale, leading to the deviation of D_H from $D_H^\star$ A similar difference is well known for IP on uncorrelated substrates in two dimensions [3]. In three dimensions, trapping occurs rarely, and no such global effect of the trapping rule on the cluster dimensionality should be expected.

The effect of the trapping rule on two-dimensional substrates is related to the dynamics of the IP process. The dynamics may be expected to be quite different from the dynamics of standard IP [29]. For example, the pair correlation function $P(r)$, giving the probability that IP cluster sites that are invaded in two subsequent steps are separated by a distance r, decays approximately as $P(r) \sim r^{-2}$ on uncorrelated substrates, for r below a cutoff length. On correlated substrates using $H = 0.5$, a much slower decay was found $[P(r) \sim r^{-\gamma}$ with $\gamma \approx 0.9]$. The cluster growth proceeded ''more smoothly,'' with prominent ''bursts'' occurring less frequently than in standard IP. For large values of H, trapping of large regions was rare and the deviation of D_H from $D_H^\star$ became small.

For low values of H, the fractal dimensionality D_H of the IP clusters appears to be close to D_{uc}, characterizing IP with trapping on uncorrelated substrates. This result is consistent with the findings of Meakin [13] mentioned in Sec. I. The multifractal substrates studied in the cited work were generated recursively and are equivalent to the self-affine ''hierarchical'' substrates used by Schmittbuhl, Vilotte, and Roux [32] in the $H \to 0$ limit.

In summary, IP with trapping on substrates with a spatially correlated threshold distribution resulting from the mapping of a self-affine surface has been studied. The fractal dimensionality of the IP clusters appears to be a tunable parameter, depending on the Hurst exponent H characterizing the threshold correlations.

ACKNOWLEDGMENTS

We gratefully acknowledge support by VISTA, a research cooperation between the Norwegian Academy of Science and Letters and Den norske stats oljeselskap a.s. (STATOIL) and by NFR, the Research Council of Norway. The work presented received support from NFR and from the Institute for Computer Applications at the University of Stuttgart through a grant of computing time.

[1] R. Lenormand and S. Bories, C.R. Acad. Sci. Paris **291**, 279 (1980).
[2] R. Chandler, J. Koplik, K. Lerman, and J. F. Willemsen, J. Fluid Mech. **119**, 249 (1982).
[3] D. Wilkinson and J. F. Willemsen, J. Phys. A **16**, 3365 (1983).
[4] N. C. Wardlaw and R. P. Taylor, Bull. Can. Petroleum Technol. **24**, 225 (1976).
[5] J. P. Hulin *et al.*, Phys. Rev. Lett. **61**, 333 (1988).
[6] A. Birovljev *et al.*, Phys. Rev. Lett. **67**, 584 (1991).
[7] M. Chaouche *et al.*, Phys. Rev. E **49**, 4133 (1994).
[8] K. J. Måløy, L. Furuberg, J. Feder, and T. Jøssang, Phys. Rev. Lett. **68**, 2161 (1992).
[9] P. Meakin, J. Feder, V. Frette, and T. Jøssang, Phys. Rev. A **46**, 3357 (1992).
[10] P. Meakin *et al.*, Physica A **191**, 227 (1992).
[11] T. A. Hewett (unpublished).
[12] P. Meakin, J. Phys. A **21**, 3501 (1988).
[13] P. Meakin, Physica A **173**, 305 (1991).
[14] A. M. Vidales *et al.*, Europhys. Lett. **36**, 259 (1996).
[15] S. R. Brown and C. H. Scholz, J. Geophys. Res. **90**, 12575 (1985).
[16] W. L. Power *et al.*, Geophys. Res. Lett. **14**, 29 (1987).
[17] W. L. Power and T. E. Tullis, J. Geophys. Res. **96**, 415 (1991).
[18] J. Schmittbuhl, S. Gentier, and S. Roux, Geophys. Res. Lett. **20**, 639 (1993).
[19] J. Schmittbuhl, F. Schmitt, and C. H. Scholz, J. Geophys. Res. **100**, 5953 (1995).
[20] J. Feder, *Fractals* (Plenum, New York, 1988).
[21] F. Plouraboue, S. Roux, J. Schmittbuhl, and J.-P. Vilotte, Fractals **3**, 113 (1995).
[22] L. Paterson, S. Painter, M. A. Knackstedt, and W. V. Pinczewski, *Patterns of Fluid Flow in Naturally Heterogeneous Rocks* (Publisher, City 1996).
[23] C. Du, C. Satik, and Y. C. Yortsos, AIChE J. **42**, 2392 (1996).
[24] M. Sahimi, AIChE J. **41**, 229 (1995).
[25] L. Paterson and S. Painter (unpublished).

[26] R. F. Voss, in *Fundamental Algorithms for Computer Graphics*, edited by R. A. Earnshaw (Springer-Verlag, Berlin, 1985), pp. 805–835.
[27] D. Saupe, in *The Science of Fractal Images*, edited by H.-O. Peitgen and D. Saupe (Springer-Verlag, Berlin, 1988), pp. 71–136.
[28] J. F. Willemsen, Phys. Rev. Lett. **52**, 2197 (1984).
[29] L. Furuberg, J. Feder, A. Aharony, and T. Jøssang, Phys. Rev. Lett. **61**, 2117 (1988).
[30] M. B. Isichenko, Rev. Mod. Phys. **64**, 961 (1992).
[31] D. Stauffer and A. Aharony, *Introduction to Percolation Theory*, 2nd ed. (Taylor & Francis, London, 1992).
[32] J. Schmittbuhl, J.-P. Vilotte, and S. Roux, J. Phys. A **26**, 6115 (1993).
[33] Z. Olami and R. Zeitak, Phys. Rev. Lett. **76**, 247 (1996).
[34] B. Nickel and D. Wilkinson, Phys. Rev. Lett. **51**, 71 (1983).
[35] D. Wilkinson and M. Barsony, J. Phys. A **17**, L129 (1984).